Supporting Information

Wadsley-Roth phase $CoNb_{11}O_{29}$ as a high-performance anode for lithium-ion batteries

Huaibing Liu, Chunhua Chen*

CAS Key Laboratory of Precision and Intelligent Chemistry, Department of Materials Science and Engineering, University of Science and Technology of China, Hefei 230026, China

* Address correspondence to cchchen@ustc.edu.cn

Prof. C.H. Chen

Department of Materials Science and Engineering

University of Science and Technology of China

Hefei 230026, P. R. China

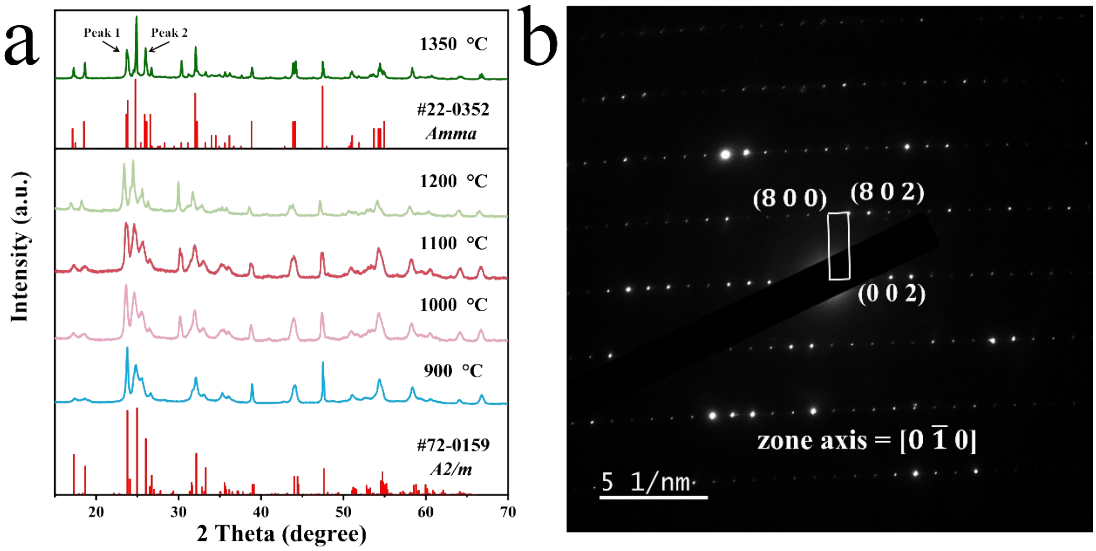

Fig. S1. (a) XRD patterns of $CoNb_{11}O_{29}$ at 900, 1000, 1100, 1200, and 1350 °C and (b) selected area electron diffraction (SAED) pattern of 1350 °C-sintered $CoNb_{11}O_{29}$.

From **Fig. S1**a we can see that there are two polymorphs of $CoNb_{11}O_{29}$. When the synthesis temperature is below 1250 °C, all of the XRD peaks can be confirmed to a $Ti_2Nb_{10}O_{29}$-type crystal structure (JCPDS#72-0159), i.e., a monoclinic shear ReO_3 crystal structure with *A2/m* space group, which is a result of the low calcination temperature. When the synthesis temperature is above 1250 °C, all of the XRD peaks match those of $FeNb_{11}O_{29}$ (JCPDS#22-0352), i.e., an orthorhombic shear ReO_3 crystal structure with *Amma* space group, which is a result of the high calcination temperature.[S1-S8] Moreover, the intensity of peak 1 is always lower than peak 2 in monoclinic phase. While in orthorhombic phase, the intensity of two peaks is very close. The SAED pattern of 1350 °C-sintered $CoNb_{11}O_{29}$ in **Fig. S1**b also demonstrates the orthorhombic phase structure.

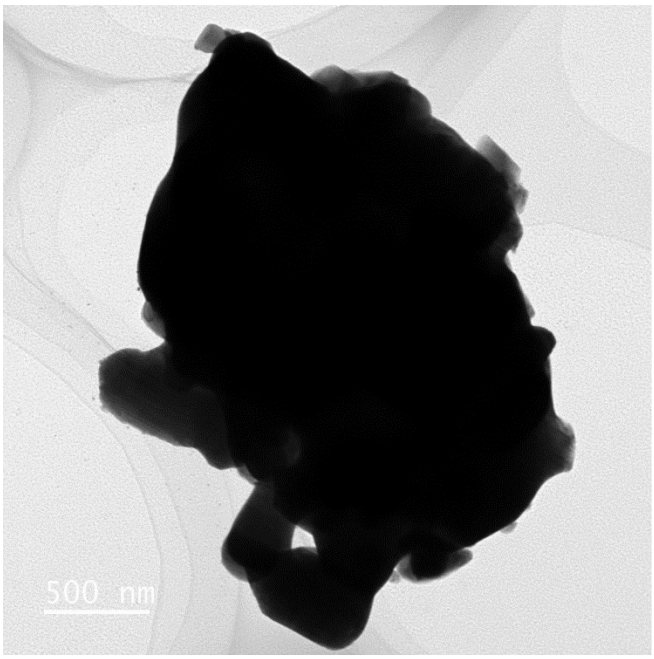

Fig. S2. TEM image of $CoNb_{11}O_{29}$.

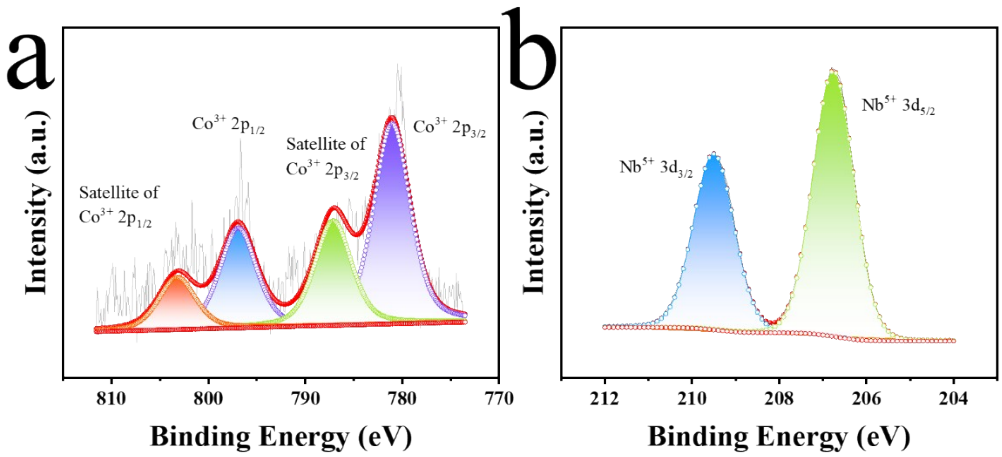

Fig. S3. Ex-situ high-resolution X-ray photoelectron spectroscopy (XPS) of $CoNb_{11}O_{29}$ powder (a) Co 2p and (b) Nb 3d spectrum.

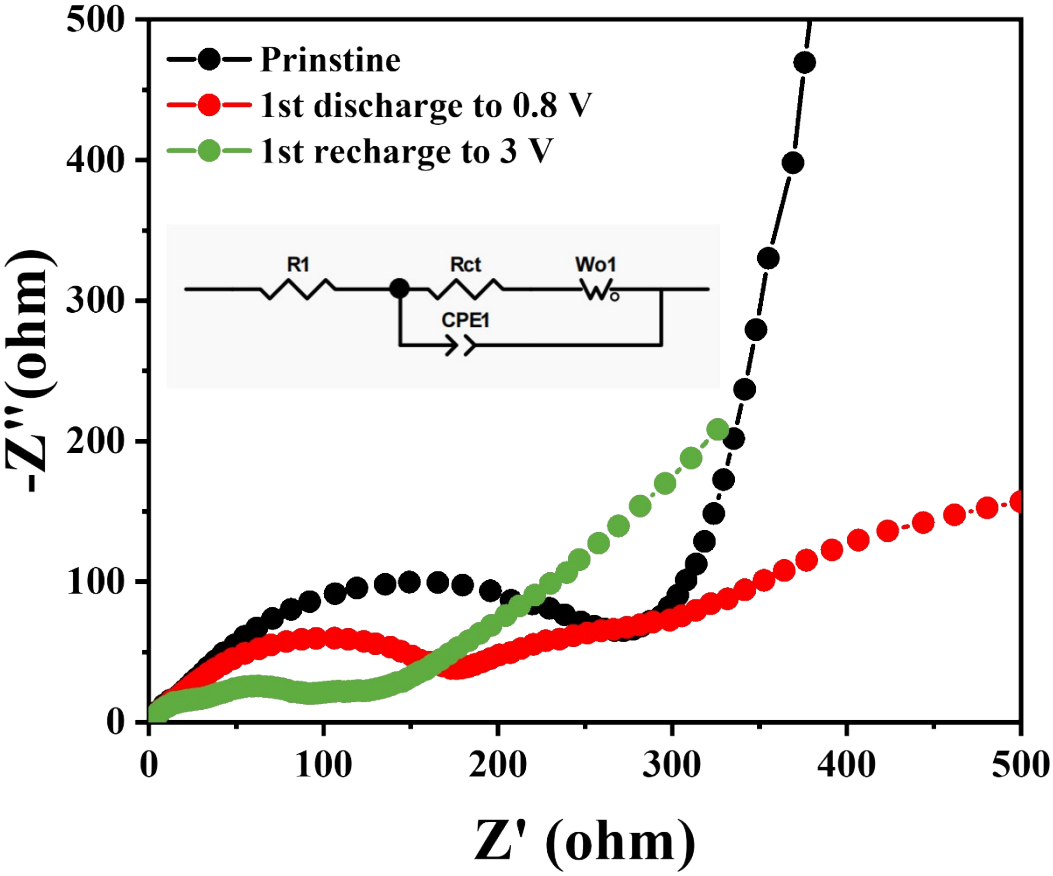

Fig. S4. Nyquist plots and the inseted equivalent circuit of different states.

As we can see from the Nyquist plots, all the states show a semicircle in the medium-frequency region, corresponding to the charge transfer resistance (R_{ct}) at the interface between the electrodes and the electrolyte. When in the open circuit state, the R_{ct} is 328 Ω. After initially discharged to 0.8 V, the R_{ct} decreases to 144 Ω. When recharged to 3V, the R_{ct} is reduced to 60 Ω. After electrode fully activated, the charge transfer resistance diminishes, resulting in faster conduction of both electrons and Li-ion during the intercalation/deintercalation process.

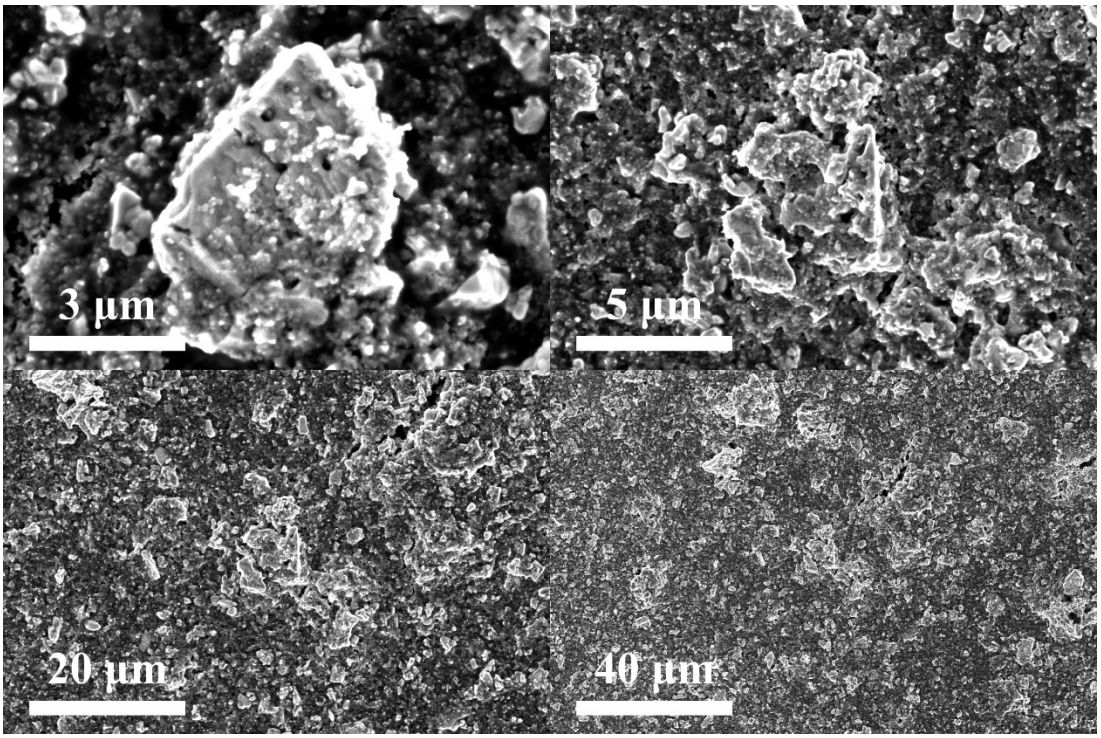

Fig. S5. SEM images of $CoNb_{11}O_{29}$ electrode after 5000 cycles.

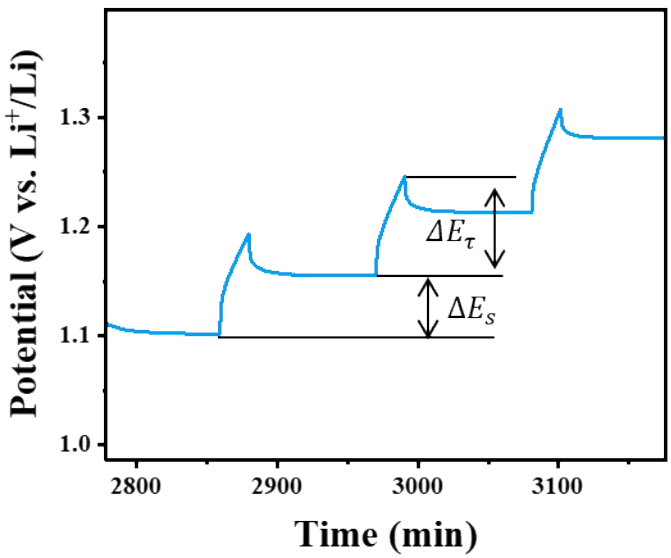

Fig. S6. The detailed charging step in GITT measurements of $CoNb_{11}O_{29}$.

The D_{Li} can be calculated via galvanostatic intermittent titration technique (GITT) curves by Fick's second law (Equation S1),

$$D_{Li} = \frac{4}{\pi\tau}\left(\frac{m_B V_m}{M_B S}\right)^2\left(\frac{\Delta E_s}{\Delta E_\tau}\right)^2\left(\tau \ll \frac{L^2}{D_{Li}}\right) \quad \text{(S1)}$$

where τ, m_B, V_m, M_B, S, and L present the time of the applied constant current, mass of the active material, molar volume of the active material, molar mass of the active material, electrode surface area, and the thickness of the electrode, respectively. ΔE_s represents the voltage difference between two adjacent equilibrium states, and ΔE_τ represents the voltage variation during the constant current pulse applied process.

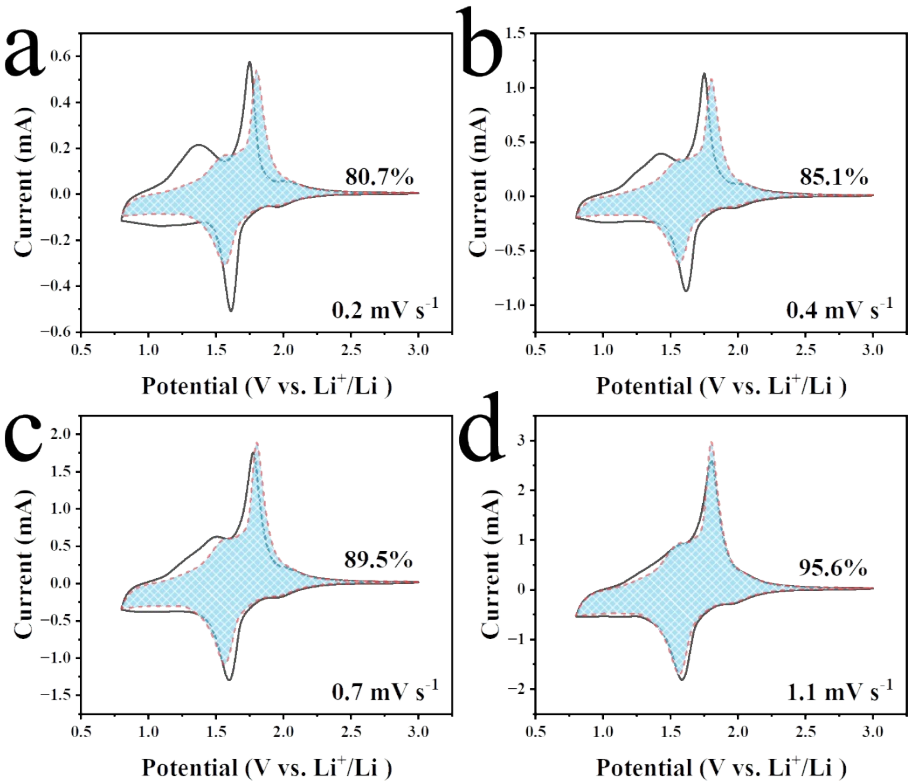

Fig. S7. Detailed CV curve at various scan rates.

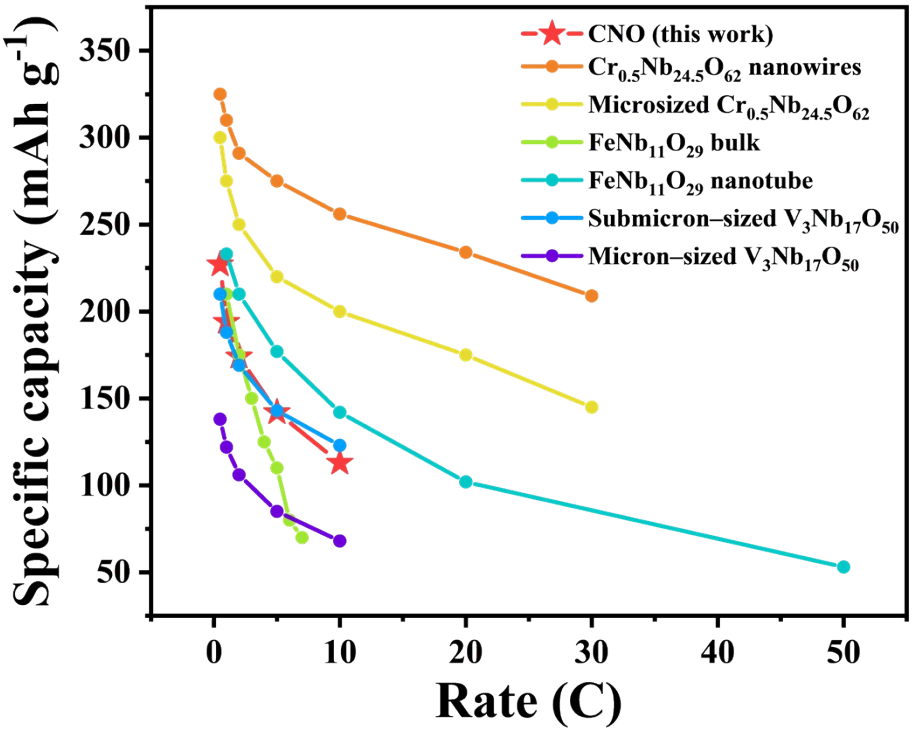

Fig. S8. The comparison of rate performance with Cr, Fe, V–doping samples.

Table S1. The fractional atomic information of $CoNb_{11}O_{29}$ with *Amma* space group.

Atom*	Symmetry	Site	*x*	*y*	*z*
M1	m	8f	0.04656	0	0.03869
M2	m	8f	0.04958	0	0.66768
M3	m	8f	0.04862	0	0.85178
M4	m	8f	0.18901	0	0.03691
M5	m	8f	0.18210	0	0.66821
M6	m	8f	0.18085	0	0.85314
O1	m2m	4c	0.25	0	0.04165
O2	m2m	4c	0.25	0	0.66732
O3	m2m	4c	0.25	0	0.85101
O4	m	8f	0.04411	0	0.56183
O5	m	8f	0.03562	0	0.14873
O6	m	8f	0.03791	0	0.75654
O7	m	8f	0.03282	0	0.34633
O8	m	8f	0.02761	0	0.94882
O9	m	8f	0.11222	0	0.03361
O10	m	8f	0.11133	0	0.66154
O11	m	8f	0.10862	0	0.85896
O12	m	8f	0.17901	0	0.56033
O13	m	8f	0.18122	0	0.14452
O14	m	8f	0.17714	0	0.75704
O15	m	8f	0.17961	0	0.35142
O16	m	8f	0.18443	0	0.94754

*M = $1/11Co^{3+} + 11/12Nb^{5+}$

Table S2. The comparison of cycling performance with Cr, Fe, V–doping samples.

Electrode materials	Cycling performance	References
$CoNb_{11}O_{29}$	**73% capacity retention after 5000 cycles at 10 C**	**This work**
Microsized $Cr_{0.5}Nb_{24.5}O_{62}$	82.4% capacity retention after 1000 cycles at 10 C	[17]
$Cr_{0.5}Nb_{24.5}O_{62}$ nanowires	92.8% capacity retention after 1000 cycles at 10 C	[17]
$FeNb_{11}O_{29}$ nanotube	71.2% capacity retention after 2000 cycles at 10 C	[18]
Submicron–sized $V_3Nb_{17}O_{50}$	91.8% capacity retention after 2000 cycles at 10 C	[19]
Micron–sized $V_3Nb_{17}O_{50}$	90.0% capacity retention after 2000 cycles at 10 C	[19]

References

[S1] P. Tabero, *Ceram.-Silik.*, 2005, **49**, 126-131.

[S2] D. Spada, M. C. Mozzati, B. Albini, P. Galinetto, I. Quinzeni, D. Capsoni and M. Bini, *Dalton Trans.*, 2018, **47**, 15816-15826.

[S3] D. Spada, I. Quinzeni and M. Bini, *Electrochim. Acta*, 2019, **296**, 938-944.

[S4] D. Spada, B. Albini, P. Galinetto, D. Versaci, C. Francia, S. Bodoardo, G. Bais and M. Bini, *Electrochim. Acta*, 2021, **393**, 139077.

[S5] D. Le Thanh, A. Guiet, E. Suard and R. Berthelot, *J. Solid State Chem.*, 2024, **330**, 124444.

[S6] R. T. Zheng, S. S. Qian, X. Cheng, H. X. Yu, N. Peng, T. T. Liu, J. D. Zhang, M. T. Xia, H. J. Zhu and J. Shu, *Nano Energy*, 2019, **58**, 399-409.

[S7] I. Pinus, M. Catti, R. Ruffo, M. M. Salamone and C. M. Mari, *Chem. Mater.*, 2014, **26**, 2203-2209.

[S8] Z. H. Lv, H. Zhu, W. W. Meng, L. C. Wei, Y. Yang, Y. F. Zhang, M. H. Ye and C. C. Li, *Appl. Phys. Rev.*, 2021, **8**, 031404.